Compact Disc Monopole Antennas for Current and Future Ultrawideband (UWB) Applications

Mohamed Nabil Srifi, Symon K. Podilchak, *Member, IEEE*, Mohamed Essaaidi, *Senior Member, IEEE*, and Yahia M. M. Antar, *Fellow, IEEE*

***Abstract*—Circular disc monopole antennas are investigated for current and future ultrawideband (UWB) applications. The studied antennas are compact and of small size (25 mm $\times$ 35 mm $\times$ 0.83 mm) with a 50-Ω feed line and offer a very simple geometry suitable for low cost fabrication and straightforward printed circuit board integration. More specifically, the impedance matching of the classic printed circular disc UWB monopole is improved by introducing transitions between the microstrip feed line and the printed disc. Two particular designs are examined using a dual and single microstrip transition. By using this simple antenna matching technique, respective impedance bandwidths ($|S_{11}| < -10$ dB) from 2.5 to 11.7 GHz and 3.5 to 31.9 GHz are obtained. Results are also compared to a classic UWB monopole with no such matching network transitions. Measured and simulated reflection coefficient curves are provided along with beam patterns, gain and group delay values as a function of frequency. The transient behavior of the studied antennas is also examined in the time domain.**

***Index Terms*—Impedance bandwidth, monopole disc antenna, ultrawideband (UWB) applications.**

I. INTRODUCTION

ULTRAWIDEBAND (UWB) technology has become a very promising solution for indoor wireless radio, imaging and radars [1], [2]. Such applications can feature very high-speed data rates, low power consumption and good immunity to multipath effects. One component in these UWB systems is the front-end antenna unit, engineered to send and receive short pulse trains with minimal distortion. Thus there has been a considerable interest by the electromagnetics community to design efficient and compact UWB antennas to operate over significant bandwidths (BWs), particularly the 3.1 to 10.6 GHz spectrum allocated by the Federal Communication Commission (FCC) in the United States for wireless transmission [3].

Manuscript received January 10, 2011; revised April 11, 2011; accepted June 02, 2011. Date of publication August 22, 2011; date of current version December 02, 2011.

M. Nabil Srifi is with the Telecommunication Systems Laboratory, National School of Applied Sciences, Ibn Tofail University, Kenitra, Morocco (e-mail: srifimn@gmail.com).

M. Essaaidi is with the Electronics and Microwaves Group, Faculty of Sciences, Abdelmalek Essaadi University, Tetouan, Morocco (e-mail: essaaidi@ieee.org).

S. K. Podilchak and Y. M. M. Antar are with Royal Military College of Canada (RMC) Kingston, ON K7K 7B4, Canada and also with Queen's University at Kingston, Kingston, ON K7L 3N6, Canada (e-mail: skp@ieee.org; antar-y@rmc.ca).

Color versions of one or more of the figures in this paper are available online at http://ieeexplore.ieee.org.

Digital Object Identifier 10.1109/TAP.2011.2165503

One of the strongest contenders in terms of achieving good impedance BWs, radiation efficiencies, and omnidirectional far field beam patterns are the circular and elliptical disc monopoles [4]–[16]. These designs can be made printed and can allow for low-cost fabrication and simple integration with associated UWB electronics. Antenna operation is generally limited within the FCC defined UWB frequency range for these antenna designs. Typical feeding techniques include simple microstrip lines [4], coplanar waveguide feeds [17], and slotted structures [18].

But with increasing demands for improved performances, higher bit rate transmission speeds, and the desire for synonymous operation with several different technologies, there may be the need for new and future UWB wireless schemes. Antenna operation could thus be required to function beyond the 10.6 GHz upper frequency band limit currently allocated by the FCC. One main design goal for these new UWB antennas is a good 50-Ω impedance match over the desired operating BW. Fortunately numerous matching and miniaturization techniques have been reported in the literature and presented concepts may prove to be helpful. Techniques include feedgap optimization [5], bevels [6], ground plane slits and shaping [12], [13], multiple feeding configurations and orientations [14], [15], variations in monopole shape [9], [16] and size reduction [19]–[21]. In addition, other important antenna design goals include minimal dispersion effects and minor group delay variations, constant gain values as a function of frequency, good impulse responses in the time domain, and in some cases, general omnidirectional radiation behavior.

In this work we study printed UWB antennas with increased impedance matching beyond the 10 GHz upper band limit typically observed for planar microstrip fed monopoles [8]. By introducing simple microstrip transitions between the 50-Ω feed line and the printed circular discs, the impedance BW of the planar monopole can be extended beyond 30 GHz. Specifically, two structures are investigated using a dual and single microstrip line transition: Designs A and B. By this added impedance matching, measured BWs ($|S_{11}| < -10$ dB) of 2.5 to 11.7 GHz and 3.5 to 31.9 GHz are respectively obtained. To evaluate antenna performances results are also compared to those of a classic UWB monopole antenna with no such matching network transitions: Design C ($|S_{11}| < -10$ dB for 3.3–10.3 GHz). Photographs of the three fabricated and measured UWB antenna structures, Designs A, B, and C, are shown in Figs. 1 and 2 while dimensions are outlined in Table I and Fig. 3. Section II discusses the design methodology and compares the operation of the proposed antennas in the

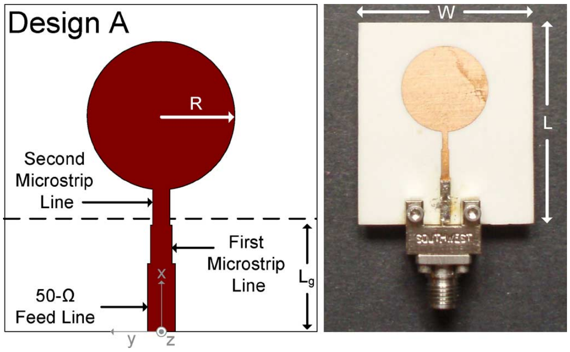

Fig. 1. Layout and photograph of the planar monopole using a dual-microstrip transition for increased 50-Ω impedance matching beyond 30 GHz.

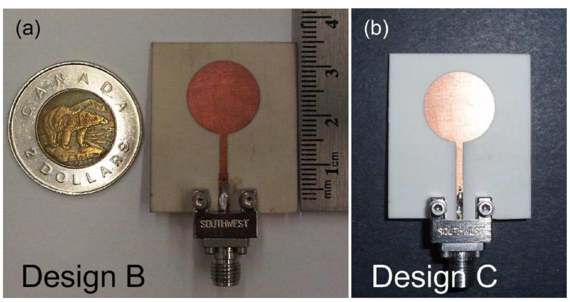

Fig. 2. Investigated planar disc UWB antennas using a single microstrip transition and just a 50-Ω feed line for comparison, (a) and (b) respectively.

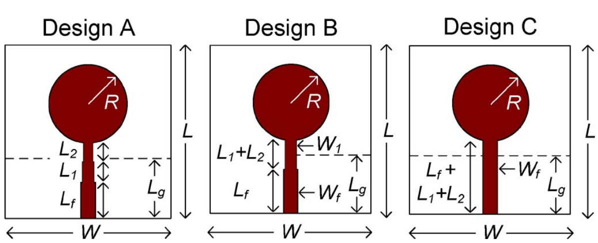

Fig. 3. Dimensions of the investigated planar disc UWB monopole antennas.

TABLE I
DIMENSIONS OF THE CIRCULAR DISC MONOPOLE ANTENNAS

Dimension		Millimeters [mm]
Width of the Substrate	W	30
Length of the Substrate	L	35
Width of the $50-\Omega$ Feed Line	W_f	1.8
Length of the $50-\Omega$ Feed Line	L_f	8
Width of the First Microstrip Line	W_1	1.4
Length of the First Microstrip Line	L_1	5
Width of the Second Microstrip Line	W_2	1
Width of the Second Microstrip Line	L_2	3
Radius of the Printed Disc	R	7.5
Length of the Partial Ground Plane	L_g	15.6
Width of the Partial Ground Plane	W_g	30
Substrate Thickness	H_{sub}	0.83

Note: Layout illustrated in Fig. 3. For Designs B and C the feed line lengths, L_1 and L_f, were respectively extended to the edge of the circular discs while all other parameters were maintained.

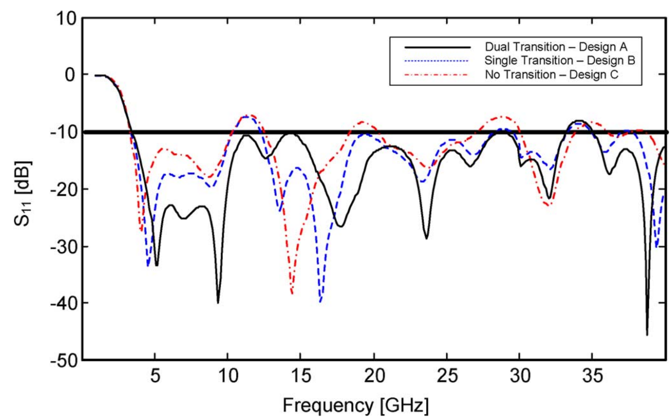

Fig. 4. Simulated reflection coefficient of the UWB planar monopoles [10].

frequency domain, while Section III describes the respective time domain responses. Results are also compared against simulations using commercial solvers in the frequency and time domains. Section IV provides a brief conclusion of the presented material.

II. ANTENNA DESIGN PRINCIPLES AND OPERATION IN THE FREQUENCY DOMAIN

The radiation mechanism of planar circular disc monopoles is an involved topic and has been investigated by many UWB antenna researchers [7], [8]. One method for analyzing such structures can be in the frequency domain where wide band monopole operation is explained by the overlapping of closely distributed minimums in the reflection coefficient, sometimes referred to as resonances [8]. This response in the broadband matching is responsible for the -10 dB impedance BW. Furthermore, at lower frequencies monopole antennas can be thought to function in an oscillating or standing wave mode, and with an increase in frequency, operation develops into a hybrid of both standing and traveling waves.

Operation at higher frequencies for these classic microstrip fed printed circular disc monopoles is generally limited to 10 GHz [4], [8]. Good antenna matching can be troublesome and very challenging to achieve in practice. Typically diminished gain and reduced radiation performances can result for these simple, single-input designs with increased ringing in the time domain due to multiple reflections along the feed line. Numerous factors contribute to this impedance mismatch such as the configuration of the ground the plane, the substrate selection, the feed line orientation, and the dimensions of the printed monopole disc. But by proper configuration of these parameters, good antenna matching may be achieved beyond 30 GHz [10]. By introducing the aforementioned microstrip transitions between the 50-Ω feed line and the printed circular discs, impedance bandwidths can be improved as shown in Figs. 4–9.

It should be mentioned that other feed line structures were investigated by the authors, but the presented microstrip transitions and ground plane configurations offered a very low cost solution for the simple antenna designs, while also offering good performance values in terms of 50-Ω impedance matching and radiation behaviors. Essentially, the dimensions of the microstrip transitions were optimized by completing a parametric analysis of W_1, L_1, W_2, and L_2 while maintaining

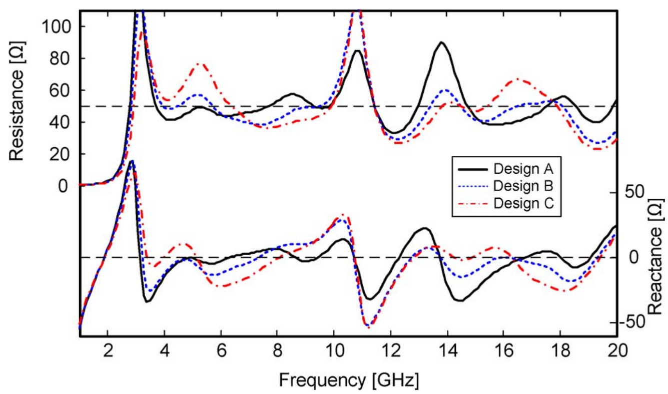

Fig. 5. Simulated input impedance, $Z_{\rm in}$, of the UWB planar monopoles.

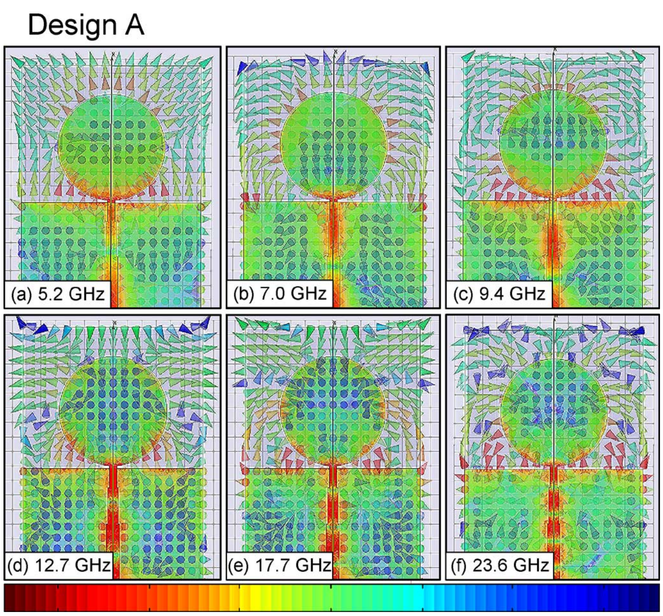

Fig. 6. Simulated current distributions (in A/m) overlaid with the electric field within the substrate at 5.2, 7.0, 9.4, 12.7, 17.7, and 23.6 GHz for Design A. The electric field (in V/m) is described by arrows with color defining field strength (red defines a maximum while blue defines a minimum, same color scale for current) and orientation defining phase along the antenna structure.

the width of input feed line, the circular shape of the disc, and the characteristics of the utilized substrate.

A. Simulated Reflection Losses & Antenna Operation

By observing the minimums in $|S_{11}|$ for the investigated antenna designs (A, B, and C), more insight into their UWB operation can be obtained [4], [8]. Simulated return loss curves are plotted in Fig. 4 and values are highlighted in Table II. At around 5 GHz the first minimums can be observed for the three monopoles. The first minimum of Design A occurs at a higher frequency (5.2 GHz) when compared to Design C (4.1 GHz). The first minimum of Design B occurs between Designs A and C (4.6 GHz). In addition, a new second minimum can be observed at 7.0 GHz for Design A and this can be thought to give rise to the very good impedance match over the 5–10 GHz range; ie. $|S_{11}| < -20$ dB. With these added transitions the minimums

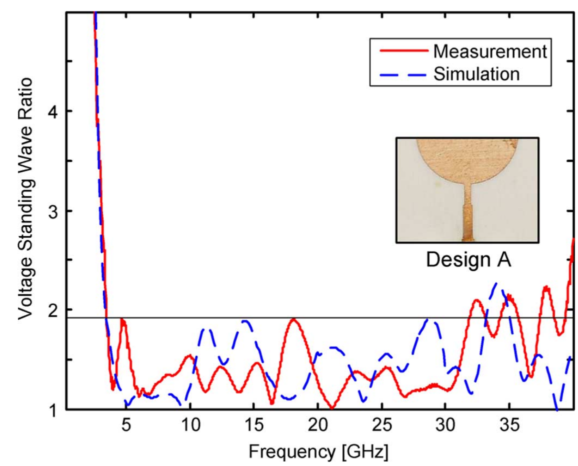

Fig. 7. VSWR of the UWB antenna, Design A, using the dual-microstrip feed configuration. A horizontal line defining a VSWR of 1.92 ($|S_{11}| = -10$ dB) is shown. Measured [Simulated] VSWR values are below 1.92 from 3.5–31.9 [3.5–28.6] GHz.

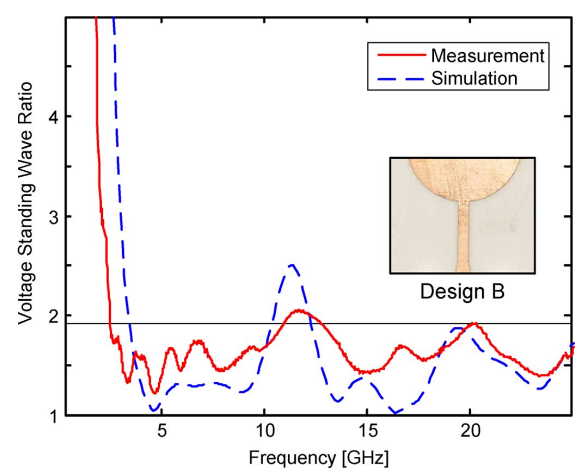

Fig. 8. VSWR of the planar monopole using only a single-microstrip feed configuration, Design B. Measured [Simulated] values are below 1.92 from 2.5–11.7 [3.2–10.5] GHz offering a 50-Ω impedance BW of 9.2 [7.3] GHz.

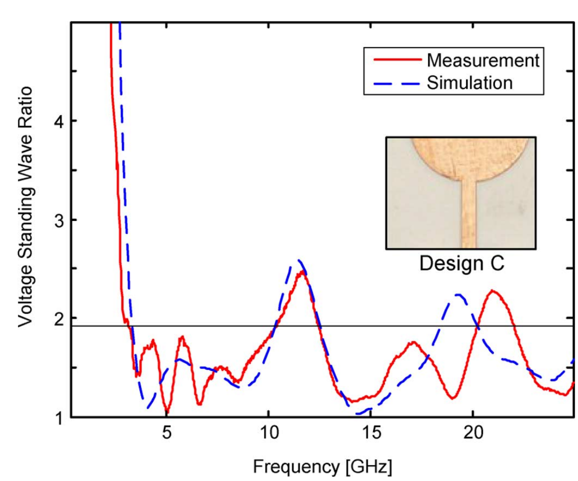

Fig. 9. VSWR of the planar monopole using only a 50-Ω feedline, Design C. Measured and simulated values are below 1.92 from 3.3–10.3 GHz offering an impedance BW of 7.0 GHz.

TABLE II
REFLECTION COEFFICIENT MINIMUMS

	1st	2nd	3rd	4th	5th	6th	7th
Freq. [GHz]							
Design A	5.2	7.0	9.4	12.7	17.7	23.6	26.7
Design B	4.6	6.7	8.9				
Design C	4.1	8.8					
$\lvert S_{11}\rvert$ [dB]							
Design A	-33.5	-25.3	-39.9	-14.7	-26.7	-28.6	-16.0
Design B	-33.5	-17.9	-19.7				
Design C	-27.7	-17.9					

Note: Simulated values shown in the matched 50-Ω impedance BW range where $|S_{11}| < -10$ dB (or VSWR < 1.92).

in $|S_{11}|$ are now more equally spaced in frequency and thus help to contribute to the good return loss values.

It should be mentioned that the 10 GHz limit of the classic monopole is extended by the dual-microstrip transition in Design A. For example, the original third minimum of Design C increased to 16.8 GHz. A new minimum is also introduced at 12.7 GHz. There is also a very good overlapping and reasonable separation for the first 5 minimums in $|S_{11}|$, giving rise to the extended impedance BW as shown in Fig. 4. It is also shown that Design A [B] $\langle$C$\rangle$ maintains a good impedance match until 28.6 [10.5] $\langle 10.3\rangle$ GHz.

Simulated input impedances "$Z_{\rm in}$" are also plotted in Fig. 5. For Design A it can be observed that $Z_{\rm in} \leq 60 \pm 30{-}\Omega$ from 3.5–10.3 GHz. This can be thought to give rise to the low reflection losses. At 10.8 and 13.8 GHz, two distinct maxima are shown in the input resistance (84.0 and 89.4-Ω, respectively), but the associated reactances are small and change from positive to negative values near these frequencies ($\mathrm{Im}\{Z_{\rm in}\} = +3.7$ and $+4.7$-Ω [-3.8 and -3.2-Ω] at 10.7 and 13.7 GHz [10.8 and 13.8 GHz]) contributing to the fourth minimum in $|S_{11}|$ at 12.7 GHz. Conversely, for both Designs B and C, the input resistances are below 32.1-Ω at this same frequency and the simulated VSWR approaches 2.5 as shown in Figs. 8 and 9. In general, the planar discs can be thought to act as a frequency dependent load in series with the added transmission line matching sections and thus the developed design strategy can be described as follows. When the real part of the input impedance is observed to be high ($\mathrm{Re}\{Z_{\rm in}\} \geq 84$-Ω), small reactances ($|\mathrm{Im}\{Z_{\rm in}\}| \leq 4$-Ω) that change sign with frequency are helpful in achieving a good antenna match. This controlled resonance was achieved by the added microstrip transitions in Design A.

Current and electric field distributions are illustrated in Fig. 6 for Design A at the first six minimums in $|S_{11}|$. Additional plots are also shown in Fig. 9 of [10] for Design A. It can be observed that the currents are mainly concentrated near the edge of the ground plane (closest to the disc), while on top of the structure currents are primarily distributed along the periphery of the disc edge and feed line [4], [8], [10]. Radiating slots can be thought to form between the lower edge of the disc and ground plane [22].

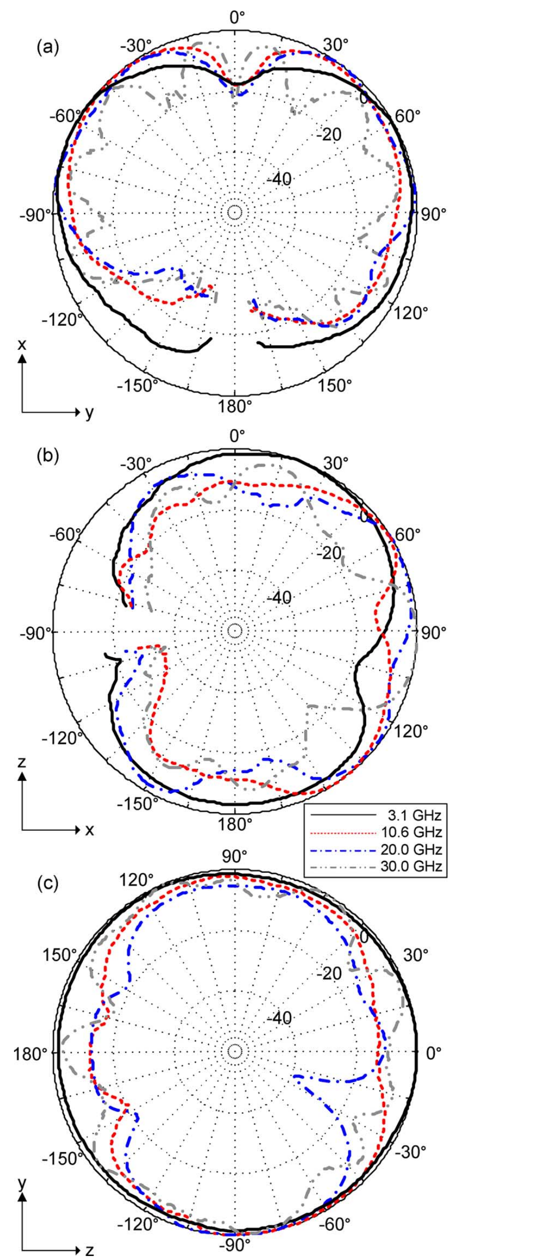

Fig. 10. Measured beam patterns for the dual transition UWB planar monopole. Normalized values are shown for Design A (Fig. 1) in dB.

Thus the radiated far fields originate from these main current distributions.

These current maxima in Fig. 6 also increase in number with frequency. For instance, at 5.2 GHz one distinct maxima can be observed at the junction of the feed line and the disc, while at 17.7 GHz five maxima are visible in total. Similar results are shown in Fig. 9 of [10]. Furthermore, these currents and electric field distributions can also signify particular modes of antenna operation. For example at 5.2 GHz the electric field is mainly directed away from the disc edges and the ground plane, while at the next minimum at 7.0 GHz, the electric field has a different orientation: from the outer edge of the disc towards the ground plane. More complex electric field distributions can also be observed in Figs. 6(c–f).

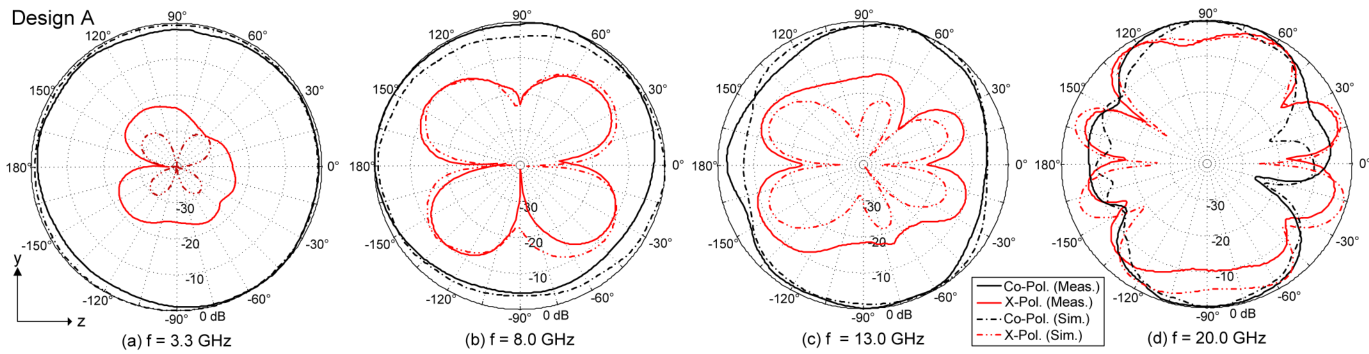

Fig. 11. Measurement and simulations of the co- and cross-polarized beam patterns in the H-plane for the monopole with the dual microstrip feed configuration.

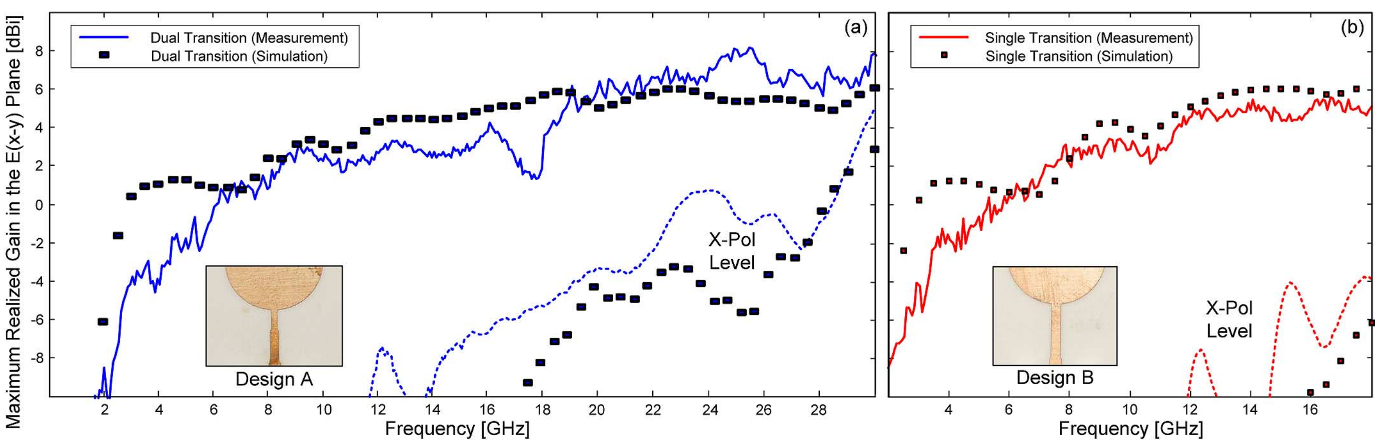

Fig. 12. Maximum observed realized gain in the $E(x-y)$ plane for the planar monopoles. (a): Design A, and (b): Design B. Similar values are observed for Design C (monopole with no transitions and just the 50-Ω feed line) as the results for the single transition structure (Design B), subplot (b) of this figure.

At higher frequencies when antenna operation has developed into a hybrid of both standing and traveling waves, phase propagation along the radial disc aperture can be inferred by observation of the current distribution (please refer to Fig. 9 of [10] at 32.0 GHz). This can signify traveling wave operation of the antenna. Moreover, at 32.0 GHz the major dimension of the antenna structure, L, is large in comparison to the free space wavelength ($\lambda_0 = 9.4$ mm, $L = 35$ mm).

B. Fabrication and Reflection Loss Measurements

The UWB circular disc monopoles (with $R = 7.5$ mm) were fabricated on 30 mm $\times$ 35 mm dielectric slabs ($\epsilon_r = 3.38$, $h = 0.83$ mm) and partial ground planes (30 mm $\times$ 15.6 mm) were maintained on the underside of the antenna substrates. The feed lines were then soldered with 50-Ω K-Connectors for reflection loss measurements in a calibrated anechoic chamber using a Anritsu 37377C Vector Network Analyzer (VNA). Results are compared to simulated values in Figs. 7–9. Good agreement in terms of the impedance match ($|S_{11}| \leq -10$ dB or VSWR$\leq$1.92) is observed. Deviations may be attributed to substrate variations over frequency, fabrication tolerances, feed connector misalignment, and difficulty in modeling the metal thicknesses near the ground planes, the circular discs, and the feed line edges due to the fabrication process. In addition, the mechanical details of the 50-Ω K Connectors were not included in the simulations in order to simplify the modeling. Regardless, the measurements and the simulation results are in agreement and this suggests that the simple microstrip feed transitions can increase the 50-Ω impedance BW of classic monopole antennas.

C. Radiation Patterns

Beam pattern measurements were completed in the frequency domain for all three monopole designs in an anechoic chamber. Measures were sampled in magnitude and phase. All trials were completed in receive mode and the appropriate calibration calculations were completed to negate cable and free space losses, chamber effects, and the contributions of the reference antennas [23]. Thus the received frequency response, $H(f, \theta, \phi)$, or normalized antenna transfer functions [24], [25] for the antennas under test were observed. Measurements were also completed in the x-y, x-z, and y-z planes and for both co- and cross-polarizations. In addition, 150 samples were recorded and averaged by the VNA for each frequency measure in an attempt to minimize any high frequency noise and multiple reflections due to cable bending and twisting.

It should be noted that some preliminary antenna gain patterns were reported earlier in [10] and agreement was observed between the measurements and simulations. Specifically, measurements were provided in the x-y and x-z planes for Designs A and B in dBi. In this work additional results are provided in Figs. 10–12. Fig. 10 shows co-polarized measurements of the

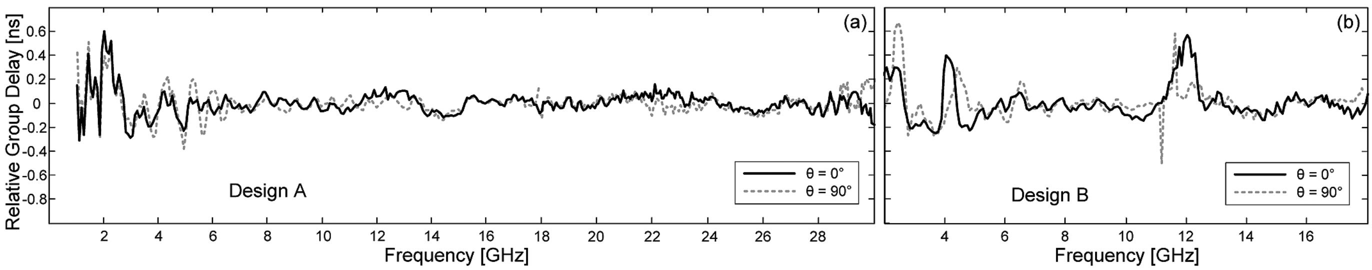

Fig. 13. Measurements of the relative group delay in the $H(x-y)$ plane for $\theta = 0^\circ$ and 90° incidence. (a): dual, and (b): single microstrip feed configuration.

TABLE III
MAXIMUM ENVELOPE VALUES

	H-Plane	E-Plane
Design A - Two Transitions	0.2306	0.2248
Design B - One Transition	0.2409	0.2230
Design C - No Transition	0.2151	0.2094

Note: All $p(\theta, \phi)$ values in m/ns.

TABLE IV
TIME DOMAIN CHARACTERISTICS AND COMPARISONS

	Measurement	Simulation
Design A - Two Transitions		
H-Plane:		
Minimum Ringing Time	121	119
Minimum FWHM	79	80
E-Plane:		
Minimum Ringing Time	98	106
Minimum FWHM	71	77
Design B - One Transition		
H-Plane:		
Minimum Ringing Time	130	121
Minimum FWHM	81	76
E-Plane:		
Minimum Ringing Time	105	120
Minimum FWHM	75	76
Design C - No Transition		
H-Plane:		
Minimum Ringing Time	121	125
Minimum FWHM	83	81
E-Plane:		
Minimum Ringing Time	97	120
Minimum FWHM	71	76

Note: All values in ps.

normalized beam patterns in the x-y, x-z, and y-z planes. Beam patterns in the H$(y{-}z)$ plane are shown in Fig. 11 and good agreement can be observed with the simulations. Measured realized gain values are also plotted in Fig. 12.

A reduction in gain of 4 dB can be observed in Fig. 12(a) for Design A at 17.5 GHz. Realized antenna gain simulations do not show a similar response. This gain decrease may correspond to the somewhat high impedance reflections (Fig. 7) also observed and centered at 17.5 GHz. However, the VSWR is still less than 1.92 in this range. For a practical UWB system this result may be acceptable. Performances could be improved by further tuning, additional microstrip transitions and the selection of a higher performance connector.

The authors wish to stress that antenna measurements were difficult to complete in the x-y and x-z planes due to the available azimuth range on the rotating antenna tower. In addition, measures in the range $\phi \in [+120^\circ, +170^\circ]$ and $\phi \in [-120^\circ, -170^\circ]$ may have reduced accuracy due the possible interference and positioning of the metallic tower and measurement cables. Absorber was also placed on the metallic antenna tower in an effort to minimize any unwanted interference. Despite these practical difficulties, results are in agreement with the simulations and a good proof of concept for the three UWB antenna structures is presented.

D. Group Delay

Small variations of the antenna phase response, or group delay τ_g[1], are important frequency domain characteristics for UWB antennas. Relative group delay values, $\tau_{g,\text{rel.}}(\omega)$, where

$$\tau_{g,\text{rel.}}(\omega) = \tau_g(\omega) - \overline{\tau_g} = \tau_g(\omega) - \frac{1}{\omega_2 - \omega_1}\int_{\omega_1}^{\omega_2} \tau_g \, d\omega \qquad (1)$$

defined as the deviation of $\tau_g(\omega)$ from the mean group delay, $\overline{\tau_g}$ [26], were plotted in Fig. 13 for Designs A and B. Minor group delay variations are observed for Design A in the operating frequency range of the antenna up to 30 GHz, while noticeably high $\tau_{g,\text{rel.}}$ values are observed for Design B between 2.0–2.8 GHz and 11.0–12.5 GHz ($|\tau_{g,\text{rel.}}| \geq 0.3$ ns). This could be caused by the high reflections observed in the VSWR of Design B below 2.5 GHz and at 12.0 GHz as respectively shown in Fig. 8. The high group delay variations from 3.9–4.7 GHz may also be related to unwanted energy storage or other dispersive effects. In brief, a similar phase response was also observed for Design C

[1]The group delay is defined as the negative derivate of the antenna phase angle with respect to frequency, $\tau_g(\omega) = -\partial\varphi/\partial\omega = -\partial\varphi/2\pi\partial f$. Small variations in group delay, defining a flat response or linear phase within a particular frequency range, suggest that waveform distortions in the time domain of transmitted or received pulses will be small; ie. a constant τ_g implies good UWB antenna operation [26]. Conversely, a nonlinear τ_g suggests unwanted resonant behavior and in the time domain this can result in ringing and unwanted oscillations[2] in the antenna impulse response, $h(t, \theta, \phi)$.

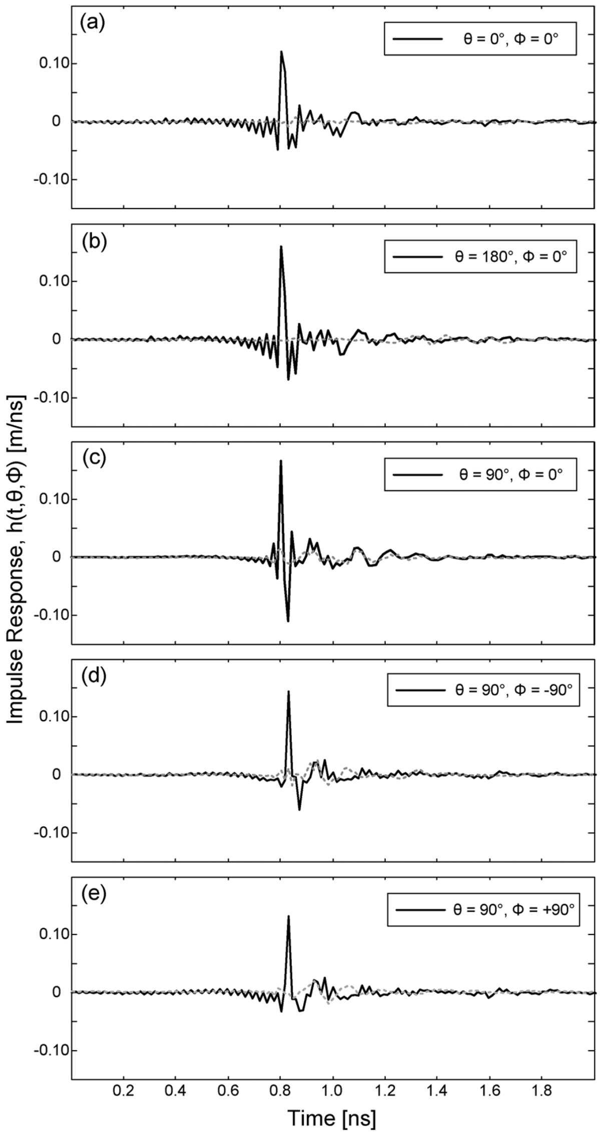

Fig. 14. Measured impulse response for the UWB monopole (Design A) with the dual microstrip feed line: Co-Pol. [X-Pol.] incidence—[– – –].

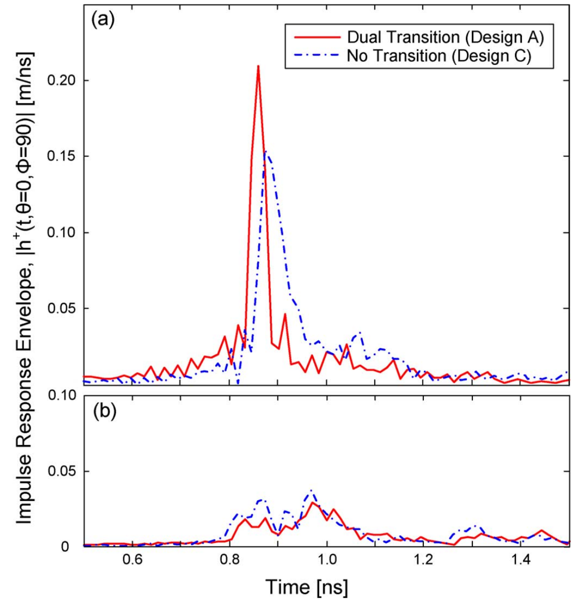

Fig. 15. Envelope of the measured impulse response ($|h^{+}(t, \theta = 0°, \phi = 90°)|$) for the dual microstrip feed configuration and the design with only a 50-Ω microstrip feedline. (a): Co-Pol response, (b): X-Pol response.

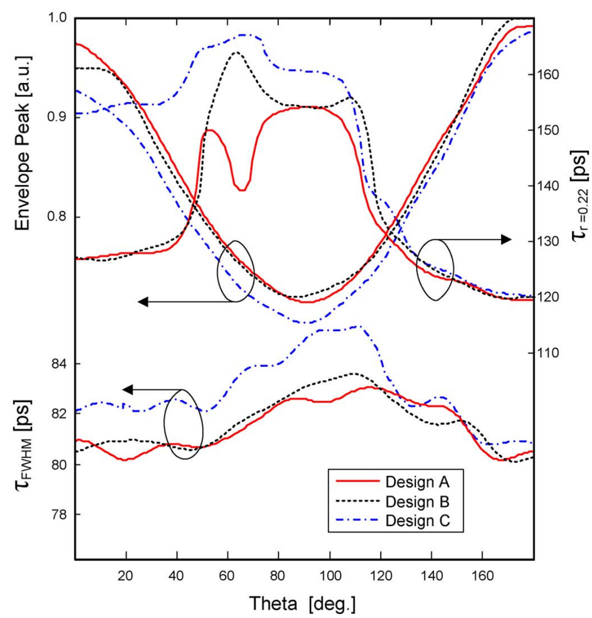

Fig. 16. Comparison of the three planar monopoles in the $H(y-z)$ plane: normalized peak envelope $|h^{+}(\theta, \phi = 90°)|$, FWHM, and ringing time.

as in Fig. 13(b). Thus these relative group delays suggest Design A has an increased performance when compared to both Designs B and C.

III. Time Domain Analysis

The previous section provided a frequency domain characterization of the examined antenna designs, but UWB systems are generally implemented using an impulse-based technology, and as such time domain effects are equally as important [7], [8]. For example, in an UWB system antenna behavior can be compared to that of a bandpass filter with constant group delay values and flat gain or amplitude responses over the entire operating BW. Signal distortion is dependent on how the spectra of transmitted and received pulses is reshaped in the time domain. This section examines important time domain characteristics of the studied UWB antennas. Results are presented in Figs. 14–20 and Tables III and IV.

A. Antenna Impulse Response

The impulse or transient responses, $h(t, \theta, \phi)$, of the investigated antennas were determined by taking the inverse Fourier transform of $H(f, \theta, \phi)$. Received frequency measures were zero padded and conjugate values were also included in the calculation to obtain full analytic responses in the time domain. Transient signals are plotted for various incident angles in Fig. 14 as a function of time for Design A. It can be observed that $h(t)$ is dependent on the angle of arrival and polarization. For example Fig. 14(c), which corresponds to the received signal at end-fire, has one main upward pulse and a second downward pulse with reduced amplitude. Oscillatory behavior[2]

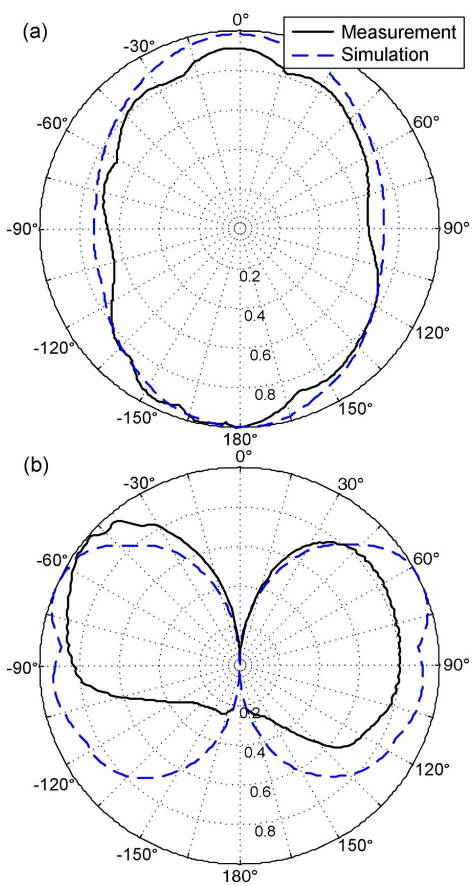

Fig. 17. Normalized peak envelope in the H- and E-planes for Design A, plots (a) and (b), respectively. Results are shown in polar form in linear units.

(or ringing) is observed after these two pulses until about 1.5 ns, suggesting increased dispersion. Reduced ringing and an increased settling time is observed for the other impulse responses.

B. Envelope of the Impulse Response, Pulse Width, & Ringing

Another method to assess the dispersive quality of UWB antennas is to calculate the envelope of the analytic impulse response, $|h^{+}(t,\theta,\phi)|$, where

$$h^{+}(t,\theta,\phi) = h(t,\theta,\phi) + j\hat{h}(t,\theta,\phi), \tag{2}$$

and $\hat{h}(t)$ refers to the Hilbert Transform of the impulse response [26]. The envelope $|h^{+}(t)|$ can be a more useful tool in assessing and quantifying antenna dispersion. Important time domain characteristics can be calculated from $|h^{+}(t)|$ including the peak value of the envelope, $p(\theta,\phi)$, the width of the observed pulse at full width half maximum (FWHM) or pulse width,

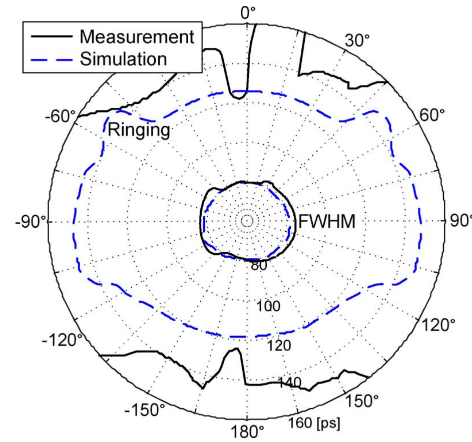

Fig. 18. Ringing time and pulse width in the H-plane for Design A.

$\tau_{\rm FWHM}$, and the duration of the ringing time,[2] τ_r. Maximum values of $p(\theta,\phi)$ are desired as this quantity can signify the amount of radiated or received power in a linear wireless system. Reduced pulse widths are also advantageous for increased data transmission rates. Ideally the FWHM should not exceed a few hundred picoseconds while the ringing time should not be more than a few pulse widths [26].

Measured values of the envelope are shown as a function of time in Fig. 15 for Designs A and C. It can be observed that the UWB monopole with the dual transitions has an increased pulse peak for the co-polarized response (0.21 m/ns) when compared to the structure with just the single microstrip line (0.15 m/ns). An increase in the pulse width can also be observed for Design C.

Maximum envelope peak values are compared in Table III for the three measured designs. It is interesting to note that Design B achieved a higher pulse peak maximum in the H plane when compared to Design A, but the opposite is true in the E plane. Reduced pulse peak values are observed for Design C, suggesting a more dispersive antenna. Simulations are also plotted in Fig. 16 for the co-polarized pulse peak along with the pulse width and ringing time (when the peak pulse is reduced to 22% of it maximum value, $\tau_{r=0.22}$). Agreement is observed with the measurements in Table III in that Design B also achieved a maximum pulse peak when compared to the two other designs at $\theta = 180^\circ$. The simulated response for $|h^{+}(t)|$ is also compared to measurements in polar form as a function of beam angle for Design A in Figs. 17 and 18. Good agreement is observed. Measured and simulated maximums of the analytic pulse peak are both at $\theta = 180^\circ$ with a general decrease at $\theta = 90^\circ$ in the H-plane.

The E-plane responses in Fig. 17(b) have a null at $\phi = 0^\circ$ and 180° suggesting more dispersive antenna behavior. This confirms the observations in Fig. 14(c) and the discussions in Section III.A regarding the increased ringing time at end-fire. Discrepancies increase near the backside of the antenna for $\phi \notin$

[2]Oscillations or the ringing after, τ_r the main pulse is defined as the quantity of time when $|h^{+}(t)|$ is reduced below a certain percentage from the peak maximum [26]. This ringing is unwanted and can be a result of energy storage or multiple reflections along the feed line and antenna structure. Energy contained in the ringing reduces the amount of radiated power, decreases peak envelope levels, and increases the pulse width of $|h^{+}(t)|$.

$[-90^\circ, +90^\circ]$ and are likely due to the aforementioned practical effects of the antenna tower and connecting cable.

The ringing time and FWHM are also compared in the H-plane in Fig. 18 as a function of angle in polar form. Agreement is shown for the observed pulse widths as mean values are both approximately 80 ps. Results are further compared in Table IV for all monopole antennas and good agreement is shown when the minimum values are observed. Differences in the ringing time are likely due to the practical challenges with such monopole antenna measurements: unwanted reflections from the anechoic chamber side walls, possible interference from the antenna test tower, and the metallic K-connector attached to the measurement cables. Despite these concerns a good proof of concept for the three UWB antenna structures is presented and agreement is observed in the measurements and simulations. Designs A and B offer reduced dispersion effects when compared to Design C.

C. Received Fidelity Due to an Incident Gaussian Waveform

To further study the measured UWB antennas fidelity estimations, F, were completed for Designs A and C using the calculated impulse responses, $h(t)$, and the fourth derivative of a template Gaussian pulse in the time domain: [24], [20]

$$s_i(t) = \alpha\left(3 - 6\left(\frac{4\pi}{\beta^2}\right)t^2 + \left(\frac{4\pi}{\beta^2}\right)^2 t^4\right) \times \exp\left\{-2\pi\left(\frac{t}{\beta}\right)^2\right\} \quad (3)$$

where $\alpha = 0.1$ and β (in ns) can characterize the pulse width of $s_i(t)$. Thus determined fidelity values can define the quality of the received waveform incident onto the antenna structure for an ideal far field source transmitting $s_i(t)$.

The power spectrum density (PSD) of the Gaussian in (3) can comply with typical FCC indoor emission mask requirements with $\beta = 0.175$ ns [24]. Furthermore, for reduced values of β sharper time domain pulses are possible along with increased spectral content in the frequency domain. For example, the normalized spectrum of this signal, $S_i(f)$, is plotted in Fig. 19 for $\beta = 0.175$ and 0.1 ns. Both signal waveforms are investigated in this work as the proposed monopole antennas could be suitable for current and future UWB systems. Moreover, the FCC could designate new spectral guidelines for future UWB systems that allow for such increased BW utilization. The Gaussian waveform of (3) (with $\beta = 0.1$ ns) could comply with forthcoming emission requirements.

Results of the fidelity estimations are shown in Fig. 20 using H-plane measurements for antenna Designs A and C. If fidelity values achieve unity, $s_i(t)$ and the received waveform, $s_r(t)$, are exactly the same in shape. This means that the antenna causes no distortion of the received pulse. Essentially, the incident signal was convolved in the time domain with the impulse response as a function of beam angle θ to determine the output waveform, $s_r(t, \theta, \phi = 90^\circ)$, at the receiving antenna terminal, mainly

$$s_r(t, \theta, \phi = 90^\circ) = s_i(t) * h(t, \theta, \phi = 90^\circ). \quad (4)$$

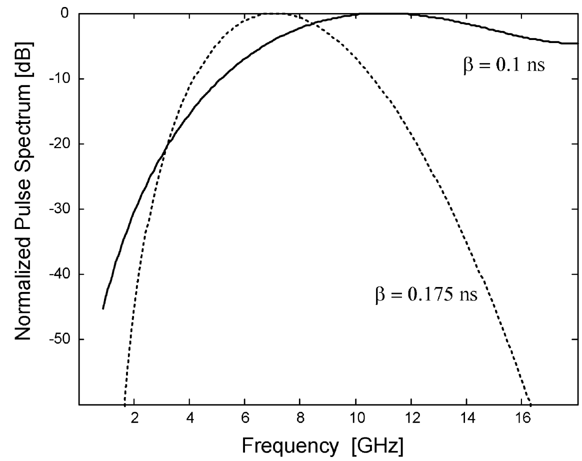

Fig. 19. Normalized spectrum for two test pulses ((3)) incident on the receiving antenna terminals with $\beta = 0.175$ ns and $\beta = 0.1$ ns.

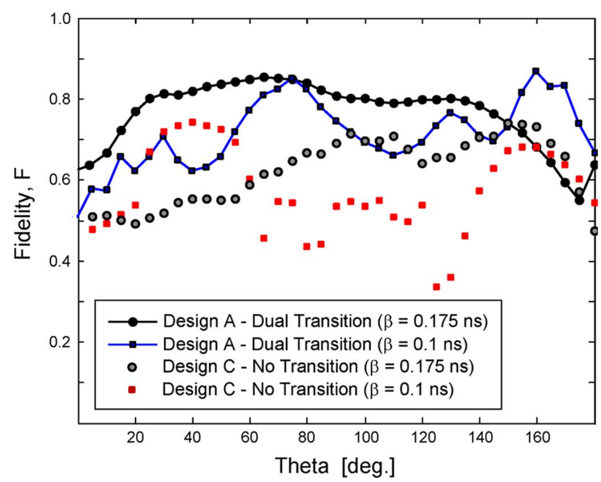

Fig. 20. Calculated fidelity for the two test pulses ($\beta = 0.175$ ns and $\beta = 0.1$ ns) incident on the dual microstrip feed configuration and the design with only a 50-Ω microstrip feedline. Results shown in the $H(y-z)$ plane using measured data for $\theta \in [0^\circ, 180^\circ]$.

By linear system theory this procedure is analogous to multiplying $S_i(f)$ and the antenna transfer functions, $H(f, \theta, \phi = 90^\circ)$ in the frequency domain and taking the Inverse Fourier Transform. For completeness both methods were verified by the authors, and as expected, identical values were observed. Fidelities were then evaluated by determining the correlation coefficient of the template Gaussian, $s_i(t)$, and the received signal $s_r(t)$. Further discussions on these procedures can be found in [20] and [24].

By analysis of Fig. 20, Design A achieved increased fidelity for both β values when compared to Design C. Average values are as follows. Design A: $\bar{F} = 0.77$ and 0.72 for $\beta = 0.175$ and 0.1 ns. Design C: $\bar{F} = 0.62$ and 0.58 for $\beta = 0.175$ and 0.1 ns. It is also interesting to note that F achieves minimum values for Design C for $\theta \in [60^\circ, 135^\circ]$. This observation is consistent with the results of Fig. 16 and the discussions of Section III.B, in that the classic monopole (Design C) can exhibit increased dispersion effects near $\theta = 90^\circ$. Calculated F values are not close to unity (likely due to the aforementioned practicalities and measurement challenges for such monopole antennas) but the expected trend is observed. Design A exhibits less distortion effects for a Gaussian waveform incident at the receiving antenna terminal when compared to Design C.

IV. Conclusion

New compact circular disc monopole antennas for UWB applications were presented and a simple technique has been introduced to improve the performance of classic UWB planar monopole antennas. Microstrip transitions, with a characteristic impedance different than 50-Ω, were arranged between the feed line and the printed discs. Calibrated measurements in an anechoic chamber show that the operating bandwidth of the proposed antennas, after introducing the single-microstrip [dual-microstrip] transition, increases from 3.3–10.3 GHz, for the classic UWB monopole, to 2.5–11.7 GHz [3.5–31.9 GHz]. Thus at most a BW of 28.4 GHz can be achieved. Improvements in these designs may be possible by additional microstrip transitions or by additional tuning techniques.

Return loss measurements are provided along with beam patterns, gain and group delay values as a function of frequency. Transient behavior of the studied UWB antennas was also presented and results suggest that the designs with the added microstrip transitions can offer reduced dispersion effects when compared to the classic planar monopole. This proposed matching technique is also very simple to introduce in practice and could be attractive for current and future UWB applications.

References

[1] K. Siwiak, "Ultra-wide band radio: Introducing a new technology," in *Proc. IEEE Veh. Technol. Conf.*, May 2001, vol. 2, pp. 1088–1093.

[2] D. G. Leeper, "Ultrawideband—The next step in short-range wireless," in *IEEE Radio Freq. Integrated Circuits Symp. Dig.*, Jun. 2003, pp. 493–496.

[3] "First Report and Order, Revision of Part 15 of the Commissions Rule Regarding Ultra Wideband Transmission Systems," Fed. Commun. Comm., FCC 02-48, Apr. 22, 2002.

[4] J. Liang, C. C. Chiau, X. Chen, and C. G. Parini, "Study of a printed circular disc monopole antenna for UWB systems," *IEEE Trans. Antennas Propag.*, vol. 53, no. 11, pp. 3500–3504, Nov. 2005.

[5] M. John and M. J. Ammann, "Optimization of impedance bandwidth for the printed rectangular monopole antenna," *Microw. Opt. Tech. Lett.*, vol. 47, no. 2, pp. 153–154, Oct. 2005.

[6] M. J. Ammann, "Control of the impedance bandwidth of wideband planar monopole antennas using a beveling technique," *Microw. Opt. Tech. Lett.*, vol. 30, no. 4, pp. 229–232, Jul. 2001.

[7] H. Schartz, *The Art and Science of Ultrawideband Antennas*. Boston, MA: Artech House, 2005.

[8] B. Allen, M. Dohler, E. Okon, W. Malik, A. Brown, and D. Edwards, *Ultra Wideband Antennas and Propagation for Communications, Radar and Imaging*. Hoboken, NJ: Wiley, 2007.

[9] A. M. Abbosh and M. E. Bialkowski, "Design of ultrawideband planar monopole antennas of circular and elliptical shape," *IEEE Trans. Antennas Propag.*, vol. 56, no. 1, pp. 17–23, Jan. 2008.

[10] M. N. Srifi, S. K. Podilchak, M. Essaaidi, and Y. M. M. Antar, "Planar circular disc monopole antennas using compact impedance matching networks for ultra-wideband (UWB) applications," in *Proc. IEEE Asia Pacific Microwave Conf.*, Dec. 2009, pp. 782–785.

[11] J. Liang, C. C. Chiau, X. Chen, and C. G. Parini, "Printed circular disc monopole antenna for ultra-wideband applications," *Electron. Lett.*, vol. 40, no. 20, pp. 1246–1248, Sep. 2004.

[12] C. Zhang and A. E. Fathy, "Development of an ultra-wideband elliptical disc planar monopole antenna with improved omnidirectional performance using a modified ground," in *Proc. IEEE Int. Antennas Propag. Symp.*, Alburqueque, NM, 2006, pp. 1689–1692.

[13] X. L. Bao and M. J. Ammann, "Investigation on UWB printed monopole antenna with rectangular slitted groundplane," *Microw. Opt. Tech. Lett.*, vol. 49, no. 7, pp. 1585–1587, Jul. 2007.

[14] E. Antonino-Daviu, M. Cabedo-Fabres, M. Ferrando-Bataller, and A. Valero-Nogueira, "Wideband double-fed planar monopole antennas," *Electron. Lett.*, vol. 39, no. 23, pp. 1635–1636, Nov. 2003.

[15] M. J. Ammann and Z. N. Chen, "An asymmetrical feed arrangement for improved impedance bandwidth of planar monopole antennas," *Microw. Opt. Tech. Lett.*, vol. 40, no. 2, pp. 156–158, Dec. 2003.

[16] J. Liu, K. P. Eselle, and S. S. Zhong, "A printed extremely wideband antenna for multi-band wiresless systems," presented at the Antennas Propagation Society Symp. (APS-URSI), Toronto, Canada, Jul. 2010.

[17] J. Liang, L. Guo, C. C. Chiau, X. Chen, and C. G. Parini, "Study of CPW-fed circular disc monopole antenna for ultra wideband applications," *IEE Proc. Microw. Antennas Propag.*, pp. 520–526, Dec. 2005.

[18] P. Li, J. Liang, and X. Chen, "Study of printed elliptical/circular slot antennas for ultrawideband applications," *IEEE Trans. Antennas Propag.*, vol. 54, no. 6, pp. 1670–1675, Jun. 2006.

[19] Q. Wu, R. Jin, J. Geng, and M. Ding, "Printed omni-directional UWB monopole antenna with very compact size," *IEEE Trans. Antennas Propag.*, vol. 56, no. 3, pp. 896–899, Mar. 2008.

[20] M. Sun, Y. P. Zhang, and Y. Lu, "Miniaturization of planar monopole antenna for ultrawideband radios," *IEEE Trans. Antennas Propag.*, vol. 58, no. 7, pp. 2420–2425, Jul. 2010.

[21] R. Zaker and A. Abdipour, "A very compact ultrawideband printed omnidirectional monopole antenna," *IEEE Antennas Wireless Propag. Lett.*, vol. 9, pp. 471–473, 2010.

[22] R. Garg, P. Bhartia, I. Bahl, and A. Ittipiboon, *Microstrip Antenna Design Handbook*. Norwood, MA: Artech House, Inc., 2001.

[23] C. A. Balanis, *Antenna Theory*, 3rd ed. Hoboken, NJ: Wiley, 2005.

[24] T. Ma and S. Jeng, "Planar miniature tapered-slot-fed annular slot antennas for ultrawide-band radios," *IEEE Trans. Antennas Propag.*, vol. 53, no. 3, pp. 1194–1202, Mar. 2005.

[25] Y. Duroc, A. Ghiotto, T. P. Vuong, and S. Tedjini, "UWB antennas: Systems with transfer function and impulse response," *IEEE Trans. Antennas Propag.*, vol. 55, no. 5, pp. 1449–1451, May 2007.

[26] W. Wiesbeck, G. Adamiuk, and C. Sturm, "Basic properties and design principles of UWB antennas," *Proc. IEEE*, vol. 97, no. 2, pp. 372–385, Feb. 2009.

Mohamed Nabil Srifi was born in Sidi Redouane Ouezzane, Morocco, in January 1978. He received the Licence de Physique degree in electronics from Ibn Tofail University, Kenitra, Morocco, in 1999, and the Deep Higher Studies Diploma DESA degree in telecommunications systems and the Ph.D. degree in electrical engineering from Abdelmalek Essaadi University, Tetuan, Morocco, in 2004 and 2009, respectively.

He is currently an Assistant Professor of electrical engineering at Ibn Tofail University, Morocco. His research interests include biological effects of radiofrequency and microwave, bio-electromagnetics, biomedical engineering and antenna design. He holds two patents on antennas for ultra-wide band applications.

Dr. Nabil Srifi is a recipient of national and international awards, and is the Vice-secretary of the Moroccan Association of Electricity, Electronics and Computers Engineering (AEECE).

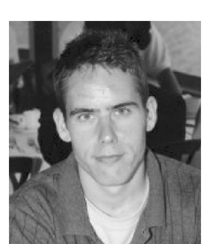

Symon K. Podilchak (S'03–M'05) received the B.A.Sc. degree from the University of Toronto, ON, Canada, in 2005. He is currently working toward the Ph.D. degree at Queen's University at Kingston (QU), ON, Canada.

He is also a Research Associate at The Royal Military College of Canada (RMC), ON, Canada. During this same period, He was a Teaching Assistant and Fellow at QU and RMC where he contributed to the development and teaching of electromagnetics and circuits based courses at the graduate and undergraduate level. He has also had experience as a computer programmer, technology investment analyst, and assisted in the design of radomes for 77 GHz automotive radar. Recent industry experience also includes modeling the radar cross-section of military vessels for high frequency surface-wave radar, professional software design and implementation for measurements in anechoic chambers, and the research and development of highly compact circularly polarized antennas for microsatellites. His current research interests include the analysis and design of planar leaky-wave antennas, metamaterials, millimetre-wave CMOS integrated circuits, UWB antennas, and periodic structures.

Mr. Podilchak has also been the recipient of more than 25 best paper awards, international travel grants, and scholarships; most notably an IEEE Antennas and Propagation Society Doctoral Research Scholarship and three Young Scientist Awards.

Mohamed Essaaidi (SM'00) is a Professor of electrical and computer engineering at Abdelmalek Essaadi University, Morocco. His research interests focus mainly on RF and microwave passive and active circuits and antennas for wireless communications and medical systems and Wireless Sensor Networks (WSN). He is the author and coauthor of more than 95 papers which appeared in refereed specialized international journals and conferences. He holds four patents on antennas for very high data rate UWB and multiband wireless communication networks and high resolution medical imaging systems. Moreover, he has supervised several Ph.D. and Masters theses and has been the principal investigator and the project manager for several international research projects dealing with different research topics concerned with his research interests mentioned above.

Prof. Essaaidi is a member of the IEEE Microwave Theory and Techniques Society, IEEE Antennas and Propagation Society, IEEE Communications Society, IEEE Computer Society and European Microwave Association. He is the Founder and the General Chair of Mediterranean Microwave Symposium (MMS) since 2000. He is also the co-Founder and the current Coordinator of the Arab Science and Technology Foundation (ASTF) RD&I network on Electrotechology. He has been also a member of the Organizing and the Scientific Committees of several international symposia and conferences dealing with topics related with RF, microwaves and Information and Communication technologies and their applications. He was the Editor of the proceedings of several international symposia and conferences and a Special Issue of the *European Microwave Association Proceedings*. He has been the Editor-in-Chief of the *International Journal of Information and Communication Technologies* since 2007. Furthermore, he has been a referee of several international journals such as the IEEE TRANSACTIONS ON MICROWAVE THEORY AND TECHNIQUES and IEEE TRANSACTIONS ON ANTENNAS AND PROPAGATION. His biography was listed in *Who's Who in The World* in 1999.

Yahia M. M. Antar (S'73–M'76–SM'85–F'00) received the B.Sc. (Hons.) degree from Alexandria University, Alexandria, Egypt, in 1966, and the M.Sc. and Ph.D. degrees from the University of Manitoba, Winnipeg, MB, Canada, in 1971 and 1975, respectively, all in electrical engineering.

In May 1979, he joined the Division of Electrical Engineering, National Research Council of Canada, Ottawa, where he worked on polarization radar applications in remote sensing of precipitation, radio wave propagation, electromagnetic scattering and radar cross section investigations. In November 1987, he joined the staff of the Department of Electrical and Computer Engineering, Royal Military College of Canada in Kingston, where he has held the position of Professor since 1990. He has authored or coauthored over 160 journal papers and 300 Conference papers, and holds several patents.

Dr. Antar is a Fellow of the IEEE and the Engineering Institute of Canada (FEIC). He is an Associate Editor (Features) of the *IEEE Antennas and Propagation Magazine* and served as Associate Editor of the IEEE TRANSACTIONS ON ANTENNAS AND PROPAGATION, *IEEE Antennas and Wireless Propagation*, and a member of the Editorial Board of the *RFMiCAE Journal*. In May 2002, he was awarded a Tier 1 Canada Research Chair position in Electromagnetic Engineering which has been renewed in 2009. In 2003, he received the 2003 Royal Military College Excellence in Research Prize. He was elected to the Board of the International Union of Radio Science (URSI) as Vice President in August 2008. He chaired conferences and has given plenary talks in many conferences, and supervised or co-supervised over 70 Ph.D. and M.Sc. theses at the Royal Military College and at Queens University, of which several have received the Governor General of Canada Gold Medal as well as best paper awards in major symposia. He served as the Chairman of the Canadian National Commission for Radio Science (CNC, URSI, 1999–2008), Commission B National Chair (1993–1999), holds adjunct appointment at the University of Manitoba, and has a cross appointment at Queens University in Kingston. He also serves, since November 2008, as Associate Director of the Defence and Security Research Institute (DSRI) and has been a member of the Defence Science Advisory Board (DSAB) since January 2011.